

Staggered mesh method for correlation energy calculations of solids: Second order Møller-Plesset perturbation theory

Xin Xing,[†] Xiaoxu Li,^{†,‡} and Lin Lin^{*,†,P,S}

Department of Mathematics, University of California, Berkeley, CA 94720, USA, School of Mathematical Sciences, Beijing Normal University, No.19, Xijiekouwai St, Haidian District, Beijing, 100875, P.R.China, Computational Research Division, Lawrence Berkeley National Laboratory, Berkeley, Berkeley, CA 94720, USA, and Challenge Institute for Quantum Computation, University of California, Berkeley, CA 94720, USA

E-mail: linlin@math.berkeley.edu

Abstract

The calculation of the MP2 correlation energy for extended systems can be viewed as a multi-dimensional integral in the thermodynamic limit, and the standard method for evaluating the MP2 energy can be viewed as a trapezoidal quadrature scheme. We demonstrate that existing analysis neglects certain contributions due to the non-smoothness of the integrand, and may significantly underestimate finite-size errors.

We propose a new staggered mesh method, which uses two staggered Monkhorst-Pack

^{*}To whom correspondence should be addressed

[†]Department of Mathematics, University of California, Berkeley, CA 94720, USA

[‡]School of Mathematical Sciences, Beijing Normal University, No.19, Xijiekouwai St, Haidian District, Beijing, 100875, P.R.China

^PComputational Research Division, Lawrence Berkeley National Laboratory, Berkeley, Berkeley, CA 94720, USA

^SChallenge Institute for Quantum Computation, University of California, Berkeley, CA 94720, USA

meshes for occupied and virtual orbitals, respectively, to compute the MP2 energy. We demonstrate that the staggered mesh method circumvents a significant error source in the standard method, in which certain quadrature nodes are always placed on points where the integrand is discontinuous. Numerical results indicate that the staggered mesh method can be particularly advantageous for quasi-1D systems, as well as quasi-2D and 3D systems with certain symmetries.

1 Introduction

Correlated wavefunction based methods have long been the standard in quantum chemistry for accurate solution of the many-electron Schrödinger equation in molecular systems. In recent years, they are also increasingly used for evaluating energies beyond the mean-field level in extended systems^{1–6}. In contrast to the zero dimensional molecular systems, properties in bulk solids, surfaces and other low-dimensional extended systems need to be calculated properly in the thermodynamic limit (TDL). Due to the steep increase of the computational cost with respect to the system size, reaching convergence in a brute force fashion is often beyond reach, and finite-size corrections must be applied. Common correction methods used to reduce the finite-size errors in correlation energy calculations include power-law extrapolation^{1,7–10}, structure factor extrapolation^{6,8,11}, and twist averaging^{6,9,12}.

Unless otherwise stated, throughout the paper, we assume the system extends along all three dimensions, and a standard Monkhorst-Pack (MP) mesh with $N_{\mathbf{k}}$ points sampled in the first Brillouin zone (BZ) is used. The power law extrapolation typically assumes that the finite-size error is proportional to $N_{\mathbf{k}}^{-1/3}$, $N_{\mathbf{k}}^{-1}$, or their linear combinations. The $N_{\mathbf{k}}^{-1/3}$ scaling is due to the fact that the correlation energy may inherit the $\mathcal{O}(N_{\mathbf{k}}^{-1/3})$ finite-size error in HF orbital energies⁵. The finite-size errors in the orbital energies can be reduced to $\mathcal{O}(N_{\mathbf{k}}^{-1})$ via the Madelung-constant correction^{13,14}. With this error removed, it has been argued based on structure factor analysis that the finite-size error in the correlation energy scales as $\mathcal{O}(N_{\mathbf{k}}^{-1})$ due to the omission of certain terms in the structure factor^{6,8}. The struc-

ture factor extrapolation method, as its name suggests, computes the finite-size correction by extrapolating the omitted structure factor around the Coulomb singularity. The twist averaging technique calculates and averages the structure factors, and consequently the correlation energies using a set of shifted \mathbf{k} -point meshes, and is often used as a pre-processing for power-law extrapolation and structure factor interpolation. The effectiveness of these correction methods can often be strongly system-dependent in practice.

In this paper, we focus on the finite-size error of correlation energy calculations and its correction in the simplest scenario, namely the correlation energy from the second order Møller-Plesset perturbation theory (MP2) for insulating systems (the MP2 energies for metallic systems may diverge^{2,15}). In the TDL, the MP2 energy can be expressed as an integral in the BZ. The numerical evaluation of the MP2 energy then uses a trapezoidal quadrature to replace the integral by a finite sum over the MP mesh. Correspondingly, the finite-size error in MP2 energy arises from two sources: the error of the integrand, and the error of the numerical quadrature. The first error comes from the basis set incompleteness and finite-size errors in orbitals and orbital energies, and can be reduced by various existing techniques^{1,16,17}.

The integrand of the MP2 energy calculation generally has many discontinuous points. In this paper, we demonstrate that existing structure-factor based error analysis^{6,8} neglects certain contributions due to the discontinuous behavior of the integrand, and underestimates the finite-size errors from the numerical quadrature. We show that the error of the numerical quadrature comes from the overall non-smoothness of the integrand and the improper placement of the quadrature nodes. Particularly, the standard MP2 calculation uses the same MP mesh for both occupied and virtual orbitals. This leads to the sampling of certain \mathbf{q} points (the difference between the \mathbf{k} points of an occupied-virtual orbital pair) on which the integrand is discontinuous. The error due to such improper placement of the quadrature nodes is $\mathcal{O}(N_{\mathbf{k}}^{-1})$.

We propose a simple modification to address this problem. Our staggered mesh method

uses one MP mesh for occupied orbitals, and another MP mesh shifted by half mesh size for virtual orbitals. We show that the integrand is well defined on all \mathbf{q} points in the numerical calculation, thus circumventing the need of structure factor extrapolation. We show that the finite-size error of the staggered mesh method is mainly affected by the intrinsic non-smoothness of the integrand in the MP2 calculation.

We compare the performance of the staggered mesh method and the standard method for a model problem, where the mean-field orbital energies and wavefunctions are obtained accurately from a given effective potential. We then demonstrate numerical tests on periodic H_2 dimer, and silicon in the quasi-1D, 2D and 3D bulk settings using the PySCF¹⁸ package. Our results indicate that the use of the staggered mesh can significantly accelerate the convergence towards the TDL in two scenarios: 1) quasi-1D systems, where the non-smoothness of the integrand is removable, 2) quasi-2D or 3D bulk systems with certain symmetries.

2 Theory

Let Ω be the unit cell, $|\Omega|$ be its volume, and Ω^* be the associated BZ. The Bravais lattice is denoted by \mathbb{L} and its associated reciprocal lattice is denoted by \mathbb{L}^* . The MP mesh is used for \mathbf{k} -point sampling in Ω^* and $N_{\mathbf{k}}$ denotes the total number of \mathbf{k} points. When the MP mesh contains the Γ -point, the system can be identified with a periodic supercell Ω^S with volume $|\Omega^S| = N_{\mathbf{k}} |\Omega|$. Each molecular orbital can be written as

$$\psi_{n\mathbf{k}}(\mathbf{r}) = \frac{1}{\sqrt{N_{\mathbf{k}}}} e^{i\mathbf{k}\cdot\mathbf{r}} u_{n\mathbf{k}}(\mathbf{r}) = \frac{1}{|\Omega| \sqrt{N_{\mathbf{k}}}} \sum_{\mathbf{G} \in \mathbb{L}^*} \hat{u}_{n\mathbf{k}}(\mathbf{G}) e^{i(\mathbf{k}+\mathbf{G})\cdot\mathbf{r}},$$

where n is a generic band index, and $u_{n\mathbf{k}}$ is periodic with respect to the unit cell. We also define the pair product (of the periodic components) as

$$\varrho_{n'\mathbf{k}',n\mathbf{k}}(\mathbf{r}) = u_{n'\mathbf{k}'}^*(\mathbf{r}) u_{n\mathbf{k}}(\mathbf{r}) := \frac{1}{|\Omega|} \sum_{\mathbf{G} \in \mathbb{L}^*} \hat{\varrho}_{n'\mathbf{k}',n\mathbf{k}}(\mathbf{G}) e^{i\mathbf{G}\cdot\mathbf{r}}.$$

Throughout the paper, $n \in \{i, j\}$ refers to the occupied orbital and $n \in \{a, b\}$ refers to the unoccupied orbital. The two-electron repulsion integral (ERI) tensor in the molecular orbital basis can be written as

$$\langle i\mathbf{k}_i, j\mathbf{k}_j | a\mathbf{k}_a, b\mathbf{k}_b \rangle = \frac{1}{|\Omega^S|} \sum'_{\mathbf{G} \in \mathbb{L}^*} \frac{4\pi}{|\mathbf{q} + \mathbf{G}|^2} \hat{\rho}_{i\mathbf{k}_i, a\mathbf{k}_a}(\mathbf{G}) \hat{\rho}_{j\mathbf{k}_j, b\mathbf{k}_b}(\mathbf{G}_{\mathbf{k}_i, \mathbf{k}_j}^{\mathbf{k}_a, \mathbf{k}_b} - \mathbf{G}). \quad (1)$$

Here $\mathbf{k}_a - \mathbf{k}_i =: \mathbf{q}$, and we have $\mathbf{k}_i + \mathbf{k}_j - \mathbf{k}_a - \mathbf{k}_b =: \mathbf{G}_{\mathbf{k}_i, \mathbf{k}_j}^{\mathbf{k}_a, \mathbf{k}_b} \in \mathbb{L}^*$ by crystal momentum conservation. The notation $\sum'_{\mathbf{G} \in \mathbb{L}^*}$ means that the possible term with $\mathbf{q} + \mathbf{G} = \mathbf{0}$ is excluded.

The correlation energy per unit cell, up to the levels of coupled cluster singles and doubles (CCSD), is given by

$$E_c = \frac{1}{N_{\mathbf{k}}} \sum_{ijab} \sum_{\mathbf{k}_i \mathbf{k}_j \mathbf{k}_a \mathbf{k}_b} (2 \langle i\mathbf{k}_i, j\mathbf{k}_j | a\mathbf{k}_a, b\mathbf{k}_b \rangle - \langle i\mathbf{k}_i, j\mathbf{k}_j | b\mathbf{k}_b, a\mathbf{k}_a \rangle) T_{i\mathbf{k}_i, j\mathbf{k}_j}^{a\mathbf{k}_a, b\mathbf{k}_b}, \quad (2)$$

where $\mathbf{k}_i, \mathbf{k}_j, \mathbf{k}_a, \mathbf{k}_b \in \Omega^*$. Here $T_{i\mathbf{k}_i, j\mathbf{k}_j}^{a\mathbf{k}_a, b\mathbf{k}_b} = t_{i\mathbf{k}_i, j\mathbf{k}_j}^{a\mathbf{k}_a, b\mathbf{k}_b} + t_{i\mathbf{k}_i}^{a\mathbf{k}_a} t_{j\mathbf{k}_j}^{b\mathbf{k}_b}$, and $t_{i\mathbf{k}_i}^{a\mathbf{k}_a}$ and $t_{i\mathbf{k}_i, j\mathbf{k}_j}^{a\mathbf{k}_a, b\mathbf{k}_b}$ are singles and doubles amplitudes obtained from solution of related amplitude equations. In the coupled cluster doubles (CCD) theory, we have $t_{i\mathbf{k}_i}^{a\mathbf{k}_a} = 0$, and the MP2 energy is further given by setting the doubles amplitude to

$$t_{i\mathbf{k}_i, j\mathbf{k}_j}^{a\mathbf{k}_a, b\mathbf{k}_b} = \frac{\langle a\mathbf{k}_a, b\mathbf{k}_b | i\mathbf{k}_i, j\mathbf{k}_j \rangle}{\varepsilon_{i\mathbf{k}_i} + \varepsilon_{j\mathbf{k}_j} - \varepsilon_{a\mathbf{k}_a} - \varepsilon_{b\mathbf{k}_b}}. \quad (3)$$

Note that Eq. (2) can be rewritten as

$$E_c = \frac{1}{N_{\mathbf{k}} |\Omega^S|} \sum_{ijab} \sum_{\mathbf{k}_i \mathbf{k}_j \mathbf{k}_a \mathbf{k}_b} \langle i\mathbf{k}_i, j\mathbf{k}_j | a\mathbf{k}_a, b\mathbf{k}_b \rangle \tilde{T}_{i\mathbf{k}_i, j\mathbf{k}_j}^{a\mathbf{k}_a, b\mathbf{k}_b}, \quad (4)$$

where we have absorbed the exchange term into the redefined amplitude

$$\tilde{T}_{i\mathbf{k}_i, j\mathbf{k}_j}^{a\mathbf{k}_a, b\mathbf{k}_b} = |\Omega^S| \left(2T_{i\mathbf{k}_i, j\mathbf{k}_j}^{a\mathbf{k}_a, b\mathbf{k}_b} - T_{i\mathbf{k}_i, j\mathbf{k}_j}^{b\mathbf{k}_b, a\mathbf{k}_a} \right),$$

and the scaling factor $|\Omega^S|$ ensures that each entry $\tilde{T}_{i\mathbf{k}_i,j\mathbf{k}_j}^{a\mathbf{k}_a,b\mathbf{k}_b}$ does not vanish in the TDL.

In order to write down the correlation energy in the TDL, we use the fact that both the ERI tensor and the T amplitude do not change if we replace any \mathbf{k} by $\mathbf{k} + \mathbf{G}$ for some $\mathbf{G} \in \mathbb{L}^*$. Then fixing $\mathbf{k}_i \in \Omega^*$, we may shift \mathbf{k}_a by some \mathbf{G} vector so that the difference $\mathbf{q} = \mathbf{k}_a - \mathbf{k}_i \in \Omega^*$. Similarly further fixing $\mathbf{k}_j \in \Omega^*$, we may shift \mathbf{k}_b so that $\mathbf{G}_{\mathbf{k}_i,\mathbf{k}_j}^{\mathbf{k}_a,\mathbf{k}_b} = \mathbf{0}$, i.e. $\mathbf{k}_b = \mathbf{k}_j - \mathbf{q}$. Note that this requires redefining $\hat{\rho}_{n'\mathbf{k}',n\mathbf{k}}$ to accommodate the case where \mathbf{k} is outside Ω^* . More importantly, such manipulation is only formal and is introduced to simplify the theoretical analysis. In practical calculations, we may still keep $\mathbf{k}_i, \mathbf{k}_j, \mathbf{k}_a, \mathbf{k}_b \in \Omega^*$ as in standard implementations. After such modifications, E_c in the TDL as $N_{\mathbf{k}} \rightarrow \infty$ can be concisely written as a triple integral over BZ (which is a 9-dimensional integral for 3D bulk systems):

$$E_c^{\text{TDL}} = \int_{\Omega^*} d\mathbf{q} \int_{\Omega^*} d\mathbf{k}_i \int_{\Omega^*} d\mathbf{k}_j \frac{|\Omega|}{(2\pi)^9} \sum_{ijab} \sum'_{\mathbf{G} \in \mathbb{L}^*} \frac{4\pi}{|\mathbf{q} + \mathbf{G}|^2} \hat{\rho}_{i\mathbf{k}_i,a(\mathbf{k}_i+\mathbf{q})}(\mathbf{G}) \hat{\rho}_{j\mathbf{k}_j,b(\mathbf{k}_j-\mathbf{q})}(-\mathbf{G}) \tilde{T}_{i\mathbf{k}_i,j\mathbf{k}_j}^{a(\mathbf{k}_i+\mathbf{q}),b(\mathbf{k}_j-\mathbf{q})}. \quad (5)$$

In this continuous formulation, we may also write $\sum'_{\mathbf{G} \in \mathbb{L}^*}$ simply as the regular summation $\sum_{\mathbf{G} \in \mathbb{L}^*}$ since the singularity set $\{\mathbf{q} + \mathbf{G} = \mathbf{0}, \mathbf{q} \in \Omega^*, \mathbf{G} \in \mathbb{L}^*\} = \{\mathbf{q} = \mathbf{0}, \mathbf{G} = \mathbf{0}\}$ is only an isolated point.

2.1 Error analysis

All numerical schemes for evaluating the correlation energy in the TDL amounts to approximating the triple integral (5). The quality of the numerical approximation can be affected by the following error sources: 1) The error introduced by replacing the integral (5) by a numerical quadrature (4), 2) The mean-field orbital energies $\{\varepsilon_{n\mathbf{k}}\}$ and orbitals $\{u_{n\mathbf{k}}(\mathbf{r})\}$ are not evaluated in the TDL, 3) Basis set incompleteness error, and the truncation of the virtual orbitals due to the finite size of the basis set, 4) Error in evaluating the T -amplitudes. The last three sources contribute to the errors of the integrand values used in the numerical

quadrature (4).

This paper only concerns the first error, i.e. the quadrature error. We assume that mean-field calculations are less expensive than correlation energy calculations, and the finite-size error of the orbitals and orbital energies could be reduced by using other correction methods and/or a large enough MP mesh if needed. Even when the same MP mesh is used to evaluate mean-field energies and orbitals, after the the Madelung-constant correction to the occupied orbital energies, the contribution of the finite-size from the orbital energies becomes $\mathcal{O}(N_{\mathbf{k}}^{-1})^5$. The error due to the incompleteness of the basis set error and the truncation of the virtual orbitals are more difficult to assess. Though such errors can be reduced via power-law extrapolation¹ or explicit correlation methods^{16,17}, we will not consider such improvements in this paper. We will also only consider the evaluation of the MP2 energy, where the T -amplitudes are given explicitly by orbital energies and ERIs. We will demonstrate below that even under such assumptions, the finite-size effect due to the quadrature error remains significant.

To connect to the commonly used argument in the literature^{6,8,11} to analyze the quadrature error using structure factors, we note that the structure factor $S_{\mathbf{q}}(\mathbf{G})$ corresponds to a part of the integrand in (5) as

$$S_{\mathbf{q}}(\mathbf{G}) = \int_{\Omega^*} d\mathbf{k}_i \int_{\Omega^*} d\mathbf{k}_j \frac{|\Omega|}{(2\pi)^9} \sum_{ijab} \hat{\varrho}_{i\mathbf{k}_i,a(\mathbf{k}_i+\mathbf{q})}(\mathbf{G}) \hat{\varrho}_{j\mathbf{k}_j,b(\mathbf{k}_j-\mathbf{q})}(-\mathbf{G}) \tilde{T}_{i\mathbf{k}_i,j\mathbf{k}_j}^{a(\mathbf{k}_i+\mathbf{q}),b(\mathbf{k}_j-\mathbf{q})}. \quad (6)$$

The correlation energy is then

$$E_c^{\text{TDL}} = \int_{\Omega^*} d\mathbf{q} \sum'_{\mathbf{G} \in \mathbb{L}^*} \frac{4\pi}{|\mathbf{q} + \mathbf{G}|^2} S_{\mathbf{q}}(\mathbf{G}). \quad (7)$$

We may also combine the information from the structure factors and define the integrand of Eq. (7) as

$$h(\mathbf{q}) = \sum'_{\mathbf{G} \in \mathbb{L}^*} \frac{4\pi}{|\mathbf{q} + \mathbf{G}|^2} S_{\mathbf{q}}(\mathbf{G}). \quad (8)$$

The standard MP2 calculation (4) can be interpreted as two quadrature steps in estimating each $S_{\mathbf{q}}(\mathbf{G})$ at a finite set of \mathbf{q} points and E_c^{TDL} as,

$$S_{\mathbf{q}}(\mathbf{G}) \approx \frac{|\Omega^*|^2}{N_{\mathbf{k}}^2} \sum_{\mathbf{k}_i, \mathbf{k}_j \in \mathcal{K}} \left(\frac{|\Omega|}{(2\pi)^9} \sum_{ijab} \hat{\varrho}_{i\mathbf{k}_i, a(\mathbf{k}_i + \mathbf{q})}(\mathbf{G}) \hat{\varrho}_{j\mathbf{k}_j, b(\mathbf{k}_j - \mathbf{q})}(-\mathbf{G}) \tilde{T}_{i\mathbf{k}_i, j\mathbf{k}_j}^{a(\mathbf{k}_i + \mathbf{q}), b(\mathbf{k}_j - \mathbf{q})} \right) \\ =: \tilde{S}_{\mathbf{q}}(\mathbf{G}), \quad \mathbf{q} \in \mathcal{K}_{\mathbf{q}}, \mathbf{G} \in \mathbb{L}^*, \quad (9)$$

$$E_c^{\text{TDL}} \approx \frac{|\Omega^*|}{N_{\mathbf{k}}} \sum_{\mathbf{q} \in \mathcal{K}_{\mathbf{q}}} \left(\sum'_{\mathbf{G} \in \mathbb{L}^*} \frac{4\pi}{|\mathbf{q} + \mathbf{G}|^2} \tilde{S}_{\mathbf{q}}(\mathbf{G}) \right), \quad (10)$$

where \mathcal{K} denotes the MP mesh and $\mathcal{K}_{\mathbf{q}}$ is a same-sized MP mesh containing all $\mathbf{q} \in \Omega^*$ defined as the minimum image of $\mathbf{k}_a - \mathbf{k}_i$ with $\mathbf{k}_i, \mathbf{k}_a \in \mathcal{K}$. Furthermore, $\mathcal{K}_{\mathbf{q}}$ always includes the Γ -point. These two steps apply the trapezoidal rules with uniform meshes $\mathcal{K} \times \mathcal{K}$ and $\mathcal{K}_{\mathbf{q}}$ for (6) and (7), respectively.

Note that the integrand in (7) is discontinuous at $\mathbf{q} = \mathbf{0}$ and its value at this point is indeterminate due to the term $(4\pi/|\mathbf{q}|^2)S_{\mathbf{q}}(\mathbf{0})$ with $\mathbf{G} = \mathbf{0}$. It has been argued that for $\mathbf{q} + \mathbf{G} \neq \mathbf{0}$, $S_{\mathbf{q}}(\mathbf{G})$ converges quickly, and hence the error is mainly due to the neglect of this discontinuous term from the primed summation in (10), which scales as $N_{\mathbf{k}}^{-1} \sim |\Omega^S|^{-1}$. However, such an analysis misses two factors:

1) Each $S_{\mathbf{q}}(\mathbf{G})$ in (9) also neglects certain discontinuous terms. Specifically, fixing \mathbf{q} and \mathbf{G} , the amplitude $\tilde{T}_{i\mathbf{k}_i, j\mathbf{k}_j}^{a(\mathbf{k}_i + \mathbf{q}), b(\mathbf{k}_j - \mathbf{q})}$ in the integrand for $S_{\mathbf{q}}(\mathbf{G})$ in (6) is discontinuous as a function of $(\mathbf{k}_i, \mathbf{k}_j)$ when $\mathbf{k}_j - \mathbf{k}_i - \mathbf{q} \in \mathbb{L}^*$ due to its exchange part, i.e.,

$$|\Omega_S| T_{i\mathbf{k}_i, j\mathbf{k}_j}^{b(\mathbf{k}_j - \mathbf{q}), a(\mathbf{k}_i + \mathbf{q})} = \frac{\sum'_{\mathbf{G}' \in \mathbb{L}^*} \frac{4\pi}{|\mathbf{k}_j - \mathbf{k}_i - \mathbf{q} + \mathbf{G}'|^2} \hat{\varrho}_{i\mathbf{k}_i, b(\mathbf{k}_j - \mathbf{q})}^*(\mathbf{G}') \hat{\varrho}_{j\mathbf{k}_j, a(\mathbf{k}_i + \mathbf{q})}^*(-\mathbf{G}')}{\varepsilon_{i\mathbf{k}_i} + \varepsilon_{j\mathbf{k}_j} - \varepsilon_{b(\mathbf{k}_j - \mathbf{q})} - \varepsilon_{a(\mathbf{k}_i + \mathbf{q})}}.$$

For each pair $(\mathbf{k}_i, \mathbf{k}_j)$ satisfying the relation $\mathbf{k}_j - \mathbf{k}_i - \mathbf{q} \in \mathbb{L}^*$, the exchange term above neglects the summation term associated with $\mathbf{k}_j - \mathbf{k}_i - \mathbf{q} + \mathbf{G}' = \mathbf{0}$, leading to $N_{\mathbf{k}}^{-2} \sim |\Omega^S|^{-2}$ error in the associated volume element corresponding to the multi-index $(\mathbf{k}_i, \mathbf{k}_j)$. For each $\mathbf{q} \in \mathcal{K}_{\mathbf{q}}$, there are exactly $N_{\mathbf{k}}$ such pairs $(\mathbf{k}_i, \mathbf{k}_j) \in \mathcal{K} \times \mathcal{K}$. Overall, neglecting the discontinuous terms when evaluating $\tilde{T}_{i\mathbf{k}_i, j\mathbf{k}_j}^{a(\mathbf{k}_i + \mathbf{q}), b(\mathbf{k}_j - \mathbf{q})}$ at these quadrature nodes leads to $\mathcal{O}(N_{\mathbf{k}}^{-1})$ error in

computing each $S_{\mathbf{q}}(\mathbf{G})$, and hence the additional $\mathcal{O}(N_{\mathbf{k}}^{-1})$ error in computing E_c^{TDL} .

2) The integrand of Eq. (7), i.e., $h(\mathbf{q})$, is not a smooth function, which leads to significant quadrature errors. The error of the trapezoidal rule can be generally analyzed using the Euler-Maclaurin expansion. Let δk denote the mesh size along each direction (i.e., $N_{\mathbf{k}} \sim (\delta k)^{-d}$ for systems that extend along d dimensions). Then for a periodic function with continuous derivatives up to m -th order, the quadrature error can be as small as $\mathcal{O}(\delta k^m)$. However, the integrand for E_c^{TDL} already has unbounded second order derivatives. Therefore standard error analysis predicts that the quadrature error can be $\mathcal{O}(\delta k^2) = \mathcal{O}(N_{\mathbf{k}}^{-2/3})$, or even worse, for three-dimensional systems. If so, the finite-size errors would in general be dominated by such quadrature errors. Fortunately, the points of discontinuity are isolated, and we find that the quadrature error should be $\mathcal{O}(\delta k^3) = \mathcal{O}(N_{\mathbf{k}}^{-1})$ in the worst case for three-dimensional systems. However, the analysis is much more involved than the direct application of the Euler-Maclaurin expansion. Instead it generalizes the result of Lyness¹⁹ for a class of punctured trapezoidal rules, and we will report the full analysis in a future publication. Furthermore, for systems with certain symmetries (for instance, three-dimensional systems with cubic symmetries), the smoothness condition of the integrand can be improved, which leads to quadrature error that decays faster than $\mathcal{O}(N_{\mathbf{k}}^{-1})$, and such faster decay agrees with the observations in the literature^{11,20}.

Our analysis above is also applicable to quasi-1D and quasi-2D systems, which samples \mathbf{k} points on the corresponding 1D axis and 2D plane in Ω^* , respectively. Without loss of generality we may assume the MP mesh includes \mathbf{k} points of the form $\mathbf{k} = (0, 0, k_z)$ for quasi-1D systems, and $\mathbf{k} = (0, k_y, k_z)$ for quasi-2D systems. The correlation energies of this model in the TDL can be written in an integral form similar to Eq. (5), while only changing the integration domains for $\mathbf{k}_i, \mathbf{k}_j$, and \mathbf{q} from Ω^* to the corresponding axis/plane in Ω^* . The discontinuity of the integrands in (6) and (7) described for 3D systems earlier still formally applies to this low-dimensional model. Neglecting discontinuous terms in quasi-1D and quasi-2D systems also leads to $\mathcal{O}(N_{\mathbf{k}}^{-1})$ quadrature error in the structure factor and the

MP2 energy. Furthermore, the quadrature error due to the non-smoothness of the integrand is at most $\mathcal{O}(N_k^{-1})$ for quasi-2D systems. The situation for quasi-1D system is qualitatively different. This is because the discontinuous points in quasi-1D systems are removable, i.e., by properly redefining the integrand values at these isolated points, $h(\mathbf{q})$ can become a smooth function (see the numerical examples in Figures 1 and 4). Therefore with a properly defined integrand, the quadrature error for quasi-1D systems can decay super-algebraically (i.e. the quadrature error decays asymptotically faster than $\mathcal{O}(\delta k^m)$ for any $m > 0$). Note that in practice, there is no need to find the proper integrand values at discontinuous points if no quadrature node overlaps with such points.

As an example, Figure 1 illustrates the discontinuities of $\tilde{T}_{i\mathbf{k}_i,j\mathbf{k}_j}^{a(\mathbf{k}_i+\mathbf{q}),b(\mathbf{k}_j-\mathbf{q})}$ and $h(\mathbf{q})$ with a quasi-1D model problem (details of the model are given in Section 3). According to the discussion above, such discontinuous behavior is generic in MP2 calculations. The standard MP2 calculation with any \mathbf{k} -point mesh \mathcal{K} always places some of its quadrature nodes at such points of discontinuity.

The discontinuity of $h(\mathbf{q})$ at $\mathbf{q} = \mathbf{0}$ is generally not removable in quasi-2D and 3D systems (similarly for the discontinuity of the integrand in (6) for computing $S_{\mathbf{q}}(\mathbf{G})$ and $h(\mathbf{q})$). For systems with certain symmetries, $\lim_{\mathbf{q} \rightarrow \mathbf{0}} h(\mathbf{q})$ may exist and we can redefine the value of $h(\mathbf{0})$ as this limit. The resulting modified integrand has improved smoothness and the resulting quadrature error can be $o(N_{\mathbf{k}}^{-1})$. In this case, the overall quadrature error will be dominated by improper placement of the quadrature nodes. As an example, Figure 2 illustrates the discontinuity of $h(\mathbf{q})$ obtained from two quasi-2D model problems which have an isotropic and an anisotropic Gaussian effective potential fields, respectively. The additional symmetry from the isotropic potential leads to the removable discontinuity at $\mathbf{q} = \mathbf{0}$ for $h(\mathbf{q})$, while in the anisotropic case, the values of $h(\mathbf{q})$ along the x, y axes are very different near $\mathbf{q} = \mathbf{0}$, and hence $\lim_{\mathbf{q} \rightarrow \mathbf{0}} h(\mathbf{q})$ is not well defined.

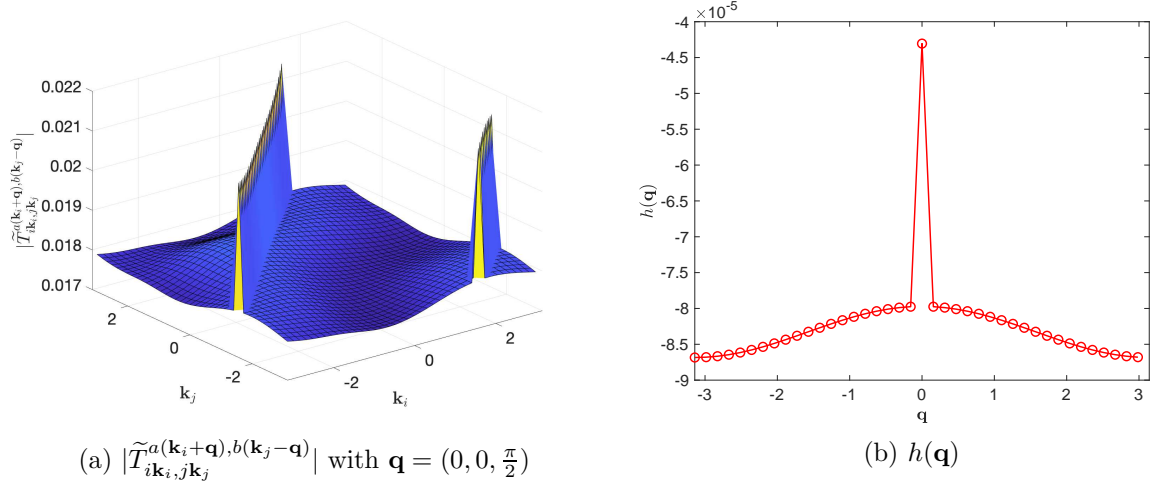


Figure 1: Illustration of discontinuities in $\tilde{T}_{i\mathbf{k}_i, j\mathbf{k}_j}^{a(\mathbf{k}_i+\mathbf{q}), b(\mathbf{k}_j-\mathbf{q})}$ and $h(\mathbf{q})$ based on a quasi-1D model problem with unit cell $[0, 1]^3$ and an anisotropic Gaussian effective potential field described in (12). All sampled \mathbf{k} points are of the form $(0, 0, k)$ with $k \in [-\pi, \pi]$. There are two lines of discontinuities in $\tilde{T}_{i\mathbf{k}_i, j\mathbf{k}_j}^{a(\mathbf{k}_i+\mathbf{q}), b(\mathbf{k}_j-\mathbf{q})}$: $k_j - k_i - \frac{\pi}{2} = 0$ and $k_j - k_i - \frac{\pi}{2} = -2\pi$.

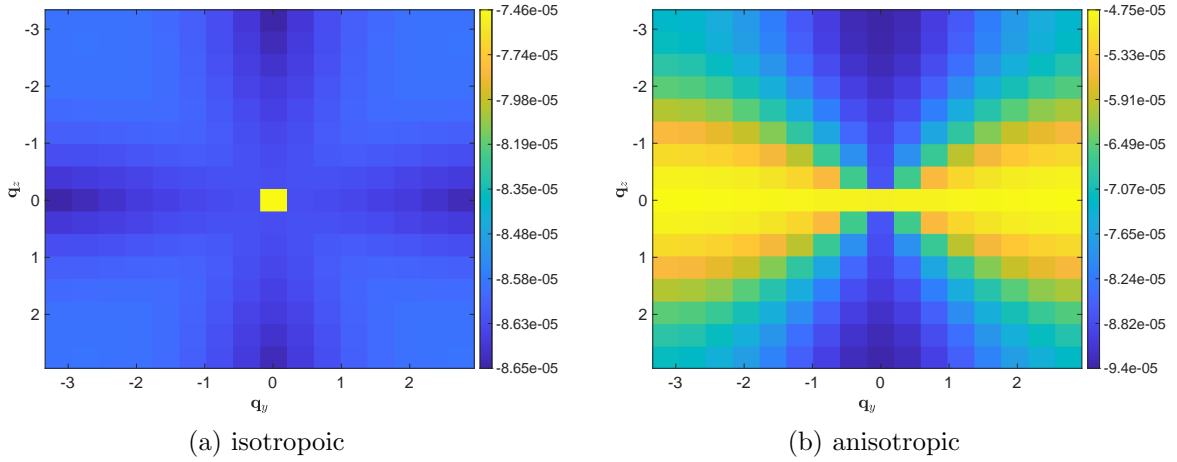


Figure 2: Illustration of discontinuities in $h(\mathbf{q})$ from two quasi-2D model problems with unit cell $[0, 1]^3$, which have an isotropic and an anisotropic Gaussian effective potential fields, respectively, as described in (12). All sampled \mathbf{q} points are of the form $(0, \mathbf{q}_y, \mathbf{q}_z)$ with $\mathbf{q}_y, \mathbf{q}_z \in [-\pi, \pi]$.

2.2 Staggered mesh method

Based on the analysis above, the potential non-smoothness of the integrand is intrinsic to the definition of E_c^{TDL} and does not depend on the choice of the quadrature scheme. However, the standard method for MP2 calculations places certain quadrature nodes on points of discontinuity of the integrand, which leads to finite-size errors of size $\mathcal{O}(N_{\mathbf{k}}^{-1})$. We propose a simple modification of the procedure to evaluate the MP2 energy, called *the staggered mesh method*. The main idea is to use an MP mesh \mathcal{K}_{occ} for occupied momentum vectors $\mathbf{k}_i, \mathbf{k}_j$, but a different, same-sized MP mesh \mathcal{K}_{vir} for virtual momentum vectors $\mathbf{k}_a, \mathbf{k}_b$, where \mathcal{K}_{vir} is obtained by shifting \mathcal{K}_{occ} with half mesh size in all extended directions to create a staggered mesh (see Figure 3). The MP2 energy is then computed as

$$E_c^{\text{staggered}} = \frac{1}{N_{\mathbf{k}} |\Omega^S|} \sum_{ijab} \sum_{\mathbf{k}_i, \mathbf{k}_j \in \mathcal{K}_{\text{occ}}} \sum_{\mathbf{k}_a, \mathbf{k}_b \in \mathcal{K}_{\text{vir}}} \langle i\mathbf{k}_i, j\mathbf{k}_j | a\mathbf{k}_a, b\mathbf{k}_b \rangle \tilde{T}_{i\mathbf{k}_i, j\mathbf{k}_j}^{a\mathbf{k}_a, b\mathbf{k}_b}, \quad (11)$$

with $N_{\mathbf{k}} = |\mathcal{K}_{\text{occ}}| = |\mathcal{K}_{\text{vir}}|$ and $|\Omega^S| = N_{\mathbf{k}}|\Omega|$.

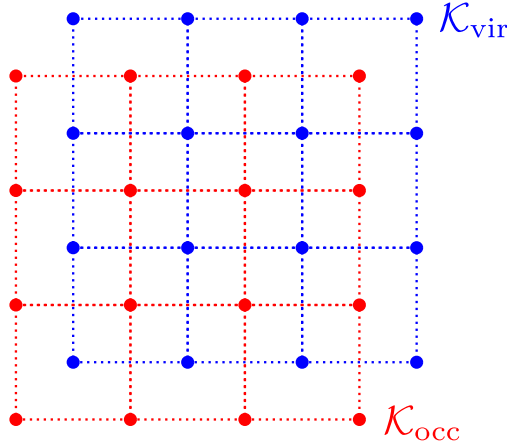


Figure 3: Illustration of the staggered meshes \mathcal{K}_{occ} and \mathcal{K}_{vir} for a quasi-2D system.

This calculation (11) can still be interpreted as a two-step numerical quadrature scheme in (9) and (10), but with a different set of quadrature nodes. The induced mesh $\mathcal{K}_{\mathbf{q}}$ in (10) shifts the Γ -centered MP mesh by half mesh size (recall that $\mathcal{K}_{\mathbf{q}}$ is the set of all possible minimum images of $\mathbf{k}_a - \mathbf{k}_i$ with $\mathbf{k}_a \in \mathcal{K}_{\text{vir}}, \mathbf{k}_i \in \mathcal{K}_{\text{occ}}$) and does not contain $\mathbf{q} = \mathbf{0}$. Recall

that in (9) for computing $S_{\mathbf{q}}(\mathbf{G})$, the integrand becomes discontinuous when $\mathbf{k}_j - \mathbf{k}_i - \mathbf{q} \in \mathbb{L}^*$. In the staggered mesh method, for each $\mathbf{q} \in \mathcal{K}_{\mathbf{q}}$, all possible values of $\mathbf{k}_j - \mathbf{k}_i - \mathbf{q}$ (for any $\mathbf{k}_i, \mathbf{k}_j \in \mathcal{K}_{\text{occ}}$) belong to $\mathcal{K}_{\mathbf{q}}$ and are always outside \mathbb{L}^* . As a result, all the defined quadrature nodes in the staggered mesh method do not overlap with any points of discontinuity of the integrand for computing $S_{\mathbf{q}}(\mathbf{G})$, $h(\mathbf{q})$, or E_c^{TDL} . This completely eliminates the first source of the error in Section 2.1, i.e., the improper placement of quadrature nodes. Figure 4 illustrates the \mathbf{q} -point mesh $\mathcal{K}_{\mathbf{q}}$ and the computed $h(\mathbf{q})$ in the standard and the staggered mesh methods for a quasi-1D model problem. We note that the staggered mesh method avoids sampling $\mathbf{q} = \mathbf{0}$ for integrating $h(\mathbf{q})$. The computed values of $h(\mathbf{q})$ are also more accurate than those computed by the standard method, as it avoids sampling discontinuous points of the integrand in (6).

The quadrature error now only comes from the second error source, i.e. lack of smoothness in corresponding integrands. For systems with certain symmetries, this error is asymptotically $o(N_{\mathbf{k}}^{-1})$ and hence the staggered mesh method exhibits significant advantages over the standard method. Another special case is quasi-1D systems, where the point of discontinuity in the integrand becomes removable, and the finite-size error of the staggered mesh method can be much smaller.

3 Numerical results

According to the discussion in Section 2.1, there are multiple factors contributing to the finite-size errors of the MP2 correlation energy. In order to focus on the contribution from the quadrature error, we will first compare the performance of the standard and the staggered mesh methods for MP2 calculations for a series of model problems with given effective potentials in Section 3.1. We then compare the performance of the two methods for periodic hydrogen and silicon systems in Section 3.2, using the PySCF software package¹⁸.

In all the following tests, the MP mesh for virtual orbitals includes the Γ point. The

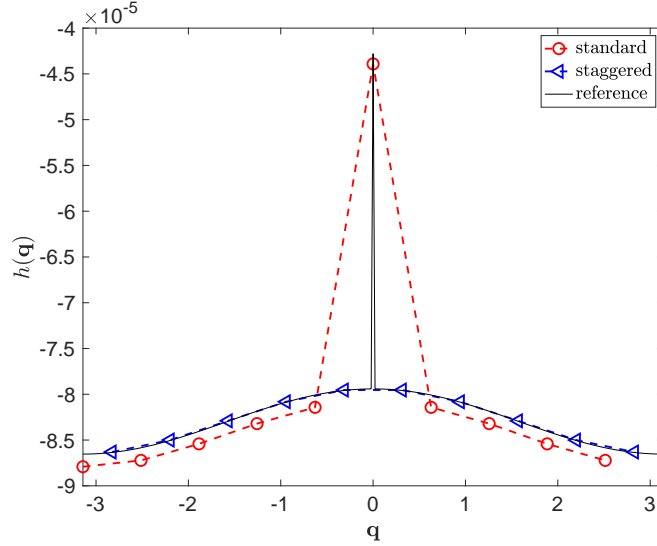


Figure 4: Illustration of $h(\mathbf{q})$ computed by the standard and the staggered mesh methods with mesh size $1 \times 1 \times 10$ for a quasi-1D model problem with unit cell $[0, 1]^3$ and an anisotropic Gaussian effective potential field described in (12). All sampled \mathbf{q} points are of the form $(0, 0, \mathbf{q}_z)$ with $\mathbf{q}_z \in [-\pi, \pi]$. The reference curve for $h(\mathbf{q})$ is computed based on the standard method with mesh size $1 \times 1 \times 300$. The discontinuity of the reference value $h(\mathbf{q} = 0)$ is removable.

standard method uses the same MP mesh for occupied orbitals. The staggered mesh method shifts the MP mesh by half mesh size for occupied orbitals. For quasi-1D, quasi-2D, and 3D systems, the MP meshes are of size $1 \times 1 \times N_{\mathbf{k}}$, $1 \times N_{\mathbf{k}}^{1/2} \times N_{\mathbf{k}}^{1/2}$, and $N_{\mathbf{k}}^{1/3} \times N_{\mathbf{k}}^{1/3} \times N_{\mathbf{k}}^{1/3}$, respectively.

3.1 Model problem

To avoid finite-size errors in orbitals and orbital energies computed by mean-field methods, we consider a model system with a (possibly anisotropic) Gaussian effective potential field. More specifically, let the unit cell be $[0, 1]^3$, and use $14 \times 14 \times 14$ planewave basis functions to discretize functions in the unit cell. The Gaussian effective potential takes the form

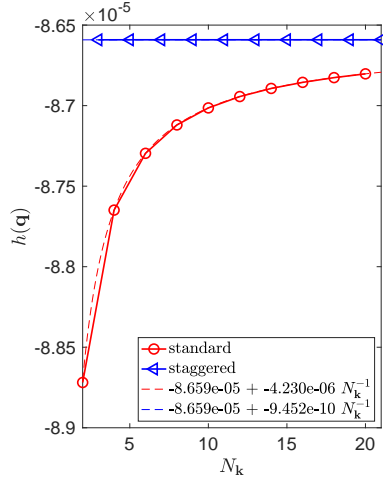
$$V(\mathbf{r}) = \sum_{\mathbf{R} \in \mathbb{L}} C \exp \left(-\frac{1}{2} (\mathbf{r} + \mathbf{R} - \mathbf{r}_0)^\top \Sigma^{-1} (\mathbf{r} + \mathbf{R} - \mathbf{r}_0) \right), \quad (12)$$

with $\mathbf{r}_0 = (0.5, 0.5, 0.5)$. For each momentum vector \mathbf{k} in Ω^* , we solve the corresponding effective Kohn-Sham equation to obtain n_{occ} occupied orbitals and n_{vir} virtual orbitals. The covariance matrix Σ controls the isotropicity of system. For the isotropic case, we choose $\Sigma = \text{diag}(0.2^2, 0.2^2, 0.2^2)$, $C = -200$, $n_{\text{occ}} = 1$, $n_{\text{vir}} = 3$. For the anisotropic case, we choose $\Sigma = \text{diag}(0.1^2, 0.2^2, 0.3^2)$, $C = -200$, $n_{\text{occ}} = 1$, $n_{\text{vir}} = 1$. For such model problems, the selected n_{vir} virtual bands are separated from the remaining virtual bands, which ensures that the MP2 correlation energy with a fixed number of virtual bands is a well defined problem. There is also a direct gap between the occupied and virtual bands in all cases.

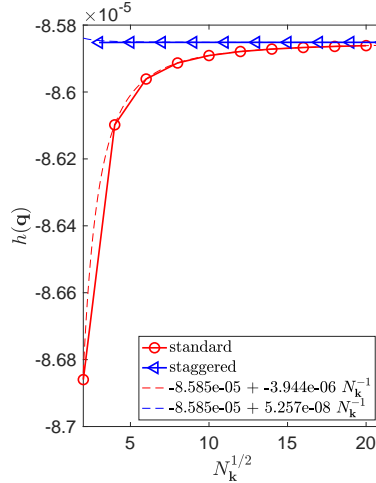
We first consider the error for estimating the integrand $h(\mathbf{q})$ in (8). For quasi-1D systems, we consider the evaluation of $h(\mathbf{q})$ at $\mathbf{q}_1 = (0, 0, \pi)$. This particular point is selected because $h(\mathbf{q}_1)$ can be directly evaluated by the standard method when $N_{\mathbf{k}}$ is even, and by the staggered mesh method when $N_{\mathbf{k}}$ is odd. Similarly, for quasi-2D and 3D systems, we consider the evaluation of $h(\mathbf{q})$ at $\mathbf{q}_2 = (0, \pi, \pi)$ and $\mathbf{q}_3 = (\pi, \pi, \pi)$, respectively.

Figure 5 demonstrates the convergence of $h(\mathbf{q})$ with respect to $N_{\mathbf{k}}$ using the standard and the staggered mesh methods. For all the systems, we find that the finite-size error of the staggered mesh method in estimating $h(\mathbf{q})$ is much smaller than that of the standard method, regardless of the dimension or the anisotropicity of the system. This suggests that the structure factor $S_{\mathbf{q}}(\mathbf{G})$ is evaluated more accurately as well by the staggered mesh method. Based on the analysis in Section 2.1, it may be surprising that the staggered mesh method significantly outperforms the standard method even in the anisotropic case. This is in fact due to the implicit symmetrization effect of the cubic cell, which reduces the error for computing $h(\mathbf{q})$.

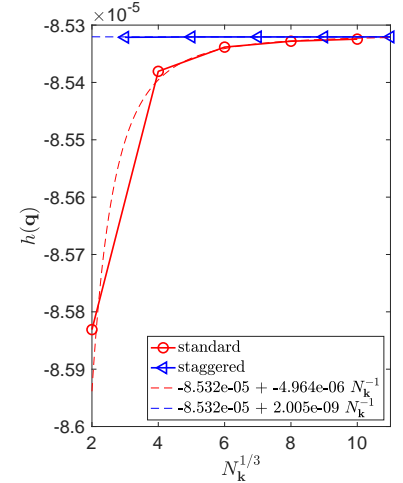
Figure 6 demonstrates the convergence of the MP2 correlation energy per unit cell computed by the standard and the staggered mesh methods for quasi-1D, quasi-2D, and 3D model systems. For quasi-1D systems, we find that the finite-size errors in the staggered mesh method decay very rapidly with respect to $N_{\mathbf{k}}$, and the curve is nearly flat. For quasi-2D and 3D model systems, the finite-size errors of the staggered mesh method are also much



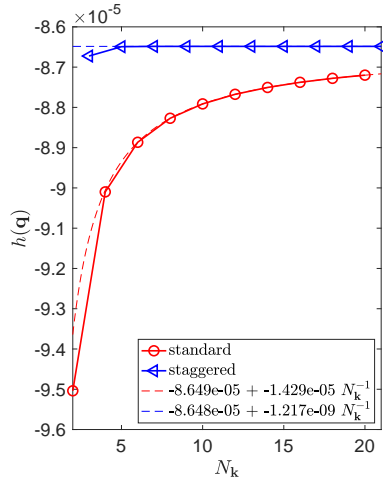
(a) Quasi-1D, isotropic



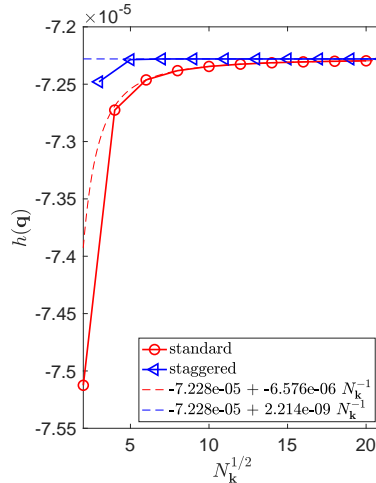
(b) Quasi-2D, isotropic



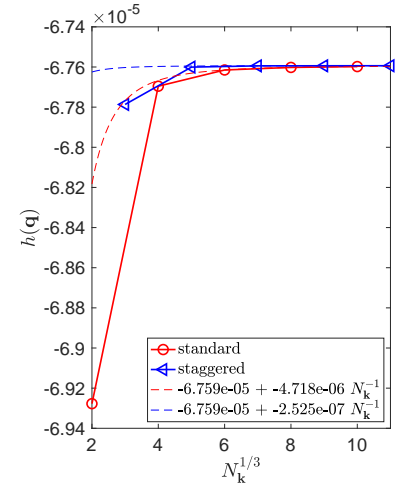
(c) 3D, isotropic



(d) Quasi-1D, anisotropic



(e) Quasi-2D, anisotropic



(f) 3D, anisotropic

Figure 5: Estimate of $h(\mathbf{q})$ at $\mathbf{q}_1/\mathbf{q}_2/\mathbf{q}_3$ using the standard and the staggered mesh methods for quasi-1D/quasi-2D/3D model systems with isotropic and anisotropic Gaussian effective potential fields. Each of these curve fittings omits the first two data points.

smaller for the isotropic systems. However, for the anisotropic systems, the convergence rates of the two methods are comparable, though the error of the staggered mesh method still exhibits a smaller preconstant.

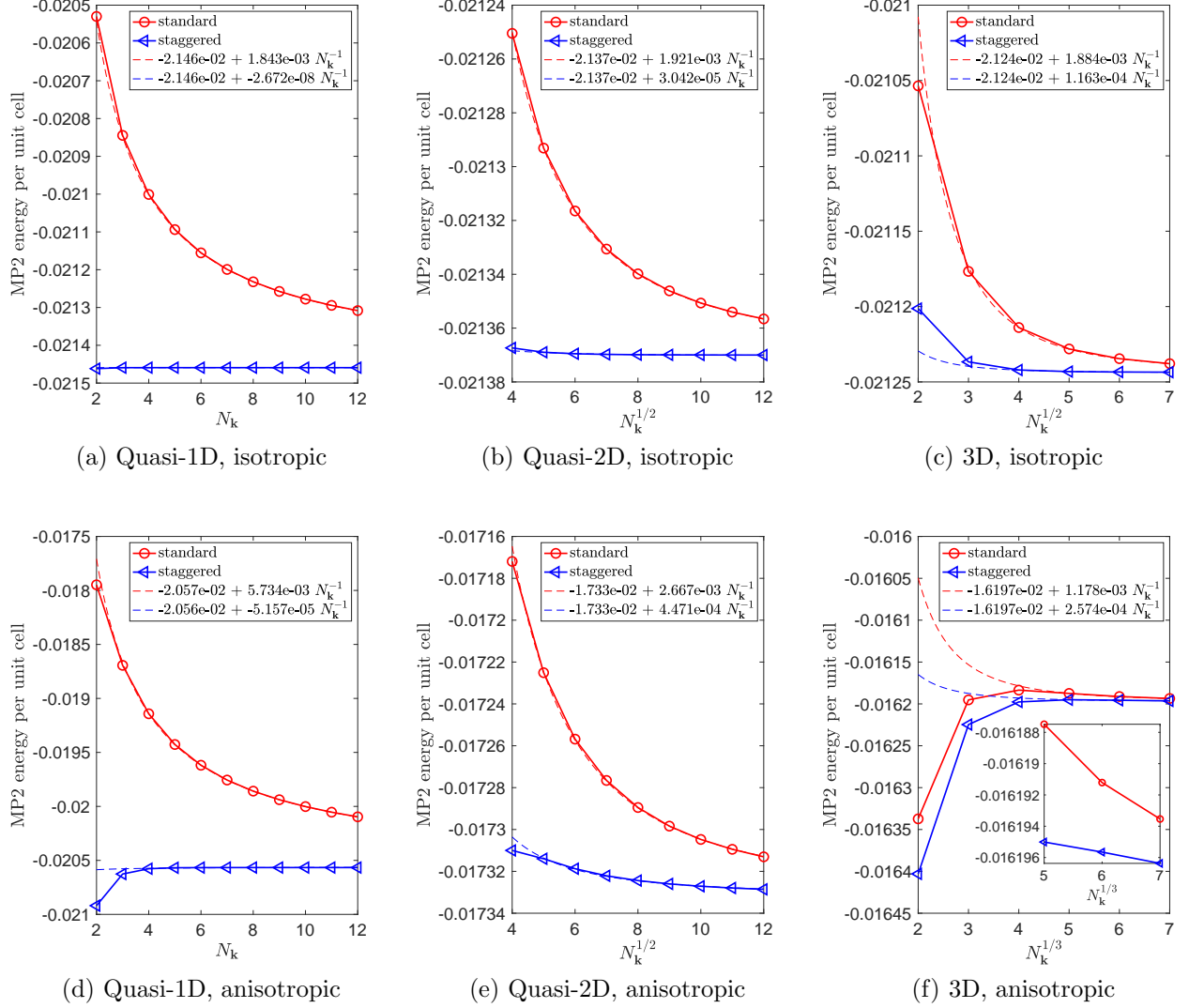


Figure 6: MP2 energy per unit cell computed by the standard and the staggered mesh methods for quasi-1D, quasi-2D, and 3D model systems with isotropic and anisotropic Gaussian effective potential fields. Each of these curve fittings omits the first two data points.

3.2 Hydrogen and silicon systems

We have implemented the staggered mesh method in the PySCF¹⁸ software package. In order to focus on the quadrature error, we perform our comparisons as follows. For 3D systems, we first compute the orbitals and orbital energies by Hartree-Fock method with a Γ -centered MP mesh of size $2N_{\mathbf{k}}^{1/3} \times 2N_{\mathbf{k}}^{1/3} \times 2N_{\mathbf{k}}^{1/3}$. Then we choose two uniform sub-meshes of size $N_{\mathbf{k}}^{1/3} \times N_{\mathbf{k}}^{1/3} \times N_{\mathbf{k}}^{1/3}$ and their associated orbitals and orbital energies to compute the MP2 energies for the staggered mesh method. We remark that this procedure is only employed to simplify our preliminary implementation in PySCF, and is not necessary in a production level computation. For the standard method, only one such sub-mesh is used. The setup of the tests for quasi-1D and quasi-2D systems is similar. Basis set gth-szv is used in all the tests below.

We consider two sets of periodic systems: hydrogen dimer, and silicon. The hydrogen dimer is placed at the center of a cubic unit cell of edge length 6 Bohr pointing in the x -direction and has separating distance 1.8 Bohr. Therefore the system is anisotropic. Silicon has a diamond cubic crystal structure, and we use a primitive unit cell containing 2 silicon atoms. Figures 7 and 8 show the MP2 energy results for quasi-1D, quasi-2D, and 3D systems for the hydrogen dimer and silicon systems.

As expected, the staggered mesh method outperforms the standard one in quasi-1D case for both systems. Note that, besides quadrature error, there is $\mathcal{O}(N_{\mathbf{k}}^{-1})$ finite-size error from those in HF orbital energies. Thus, the fitting for the staggered mesh method still uses the power law scaling of $N_{\mathbf{k}}^{-1}$. For quasi-2D and 3D cases, the staggered mesh method performs significant better than the standard one for silicon. This is likely due to the symmetry of the system that leads to improved smoothness in the integrand and thus reduces the corresponding quadrature error. In comparison, the performance of the two methods become similar for the quasi-2D and 3D hydrogen dimer systems due to the anisotropy.

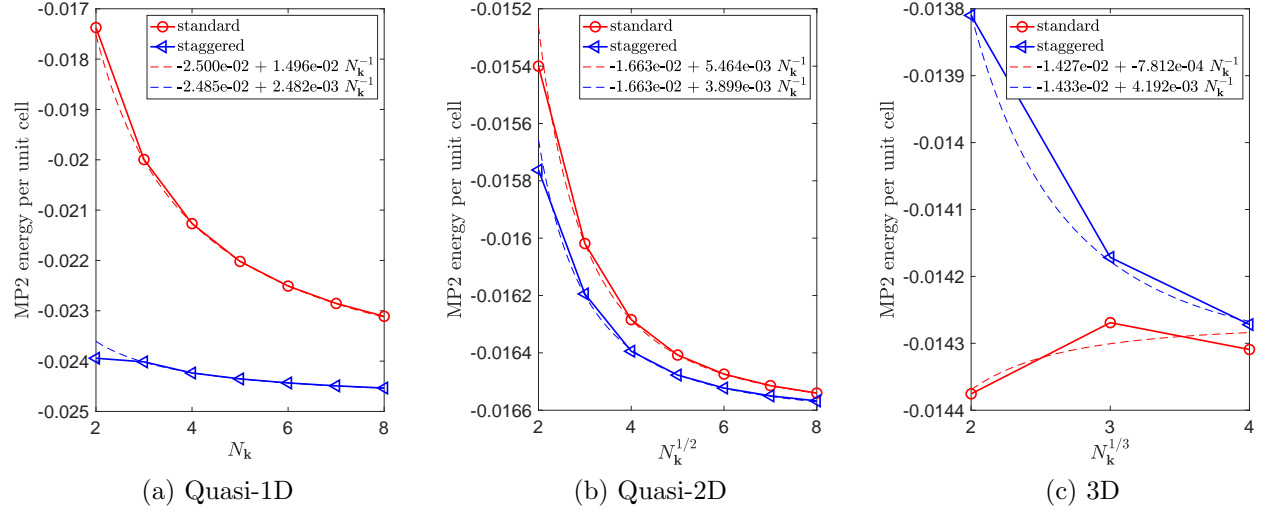


Figure 7: MP2 energy per unit cell computed by the standard and the staggered mesh methods for the periodic hydrogen dimer systems.

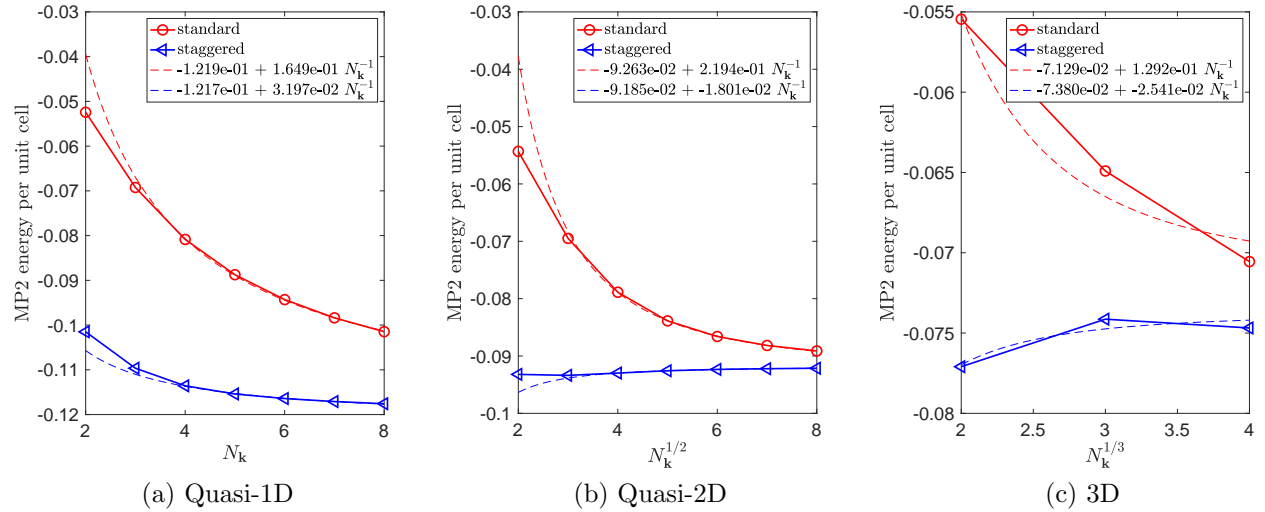


Figure 8: MP2 energy per unit cell computed by the standard and the staggered mesh methods for silicon crystal systems.

4 Conclusion

The convergence of the MP2 correlation energy towards the TDL is a fundamental question in materials science. Existing analysis in the literature focuses on the missing contribution of the structure factor $S_{\mathbf{q}}(\mathbf{G})$ at $\mathbf{q} + \mathbf{G} = \mathbf{0}$, but neglects contributions from 1) certain quadrature nodes coincide with points of discontinuity of the integrand 2) the quadrature error due to the intrinsic non-smoothness of the integrand. We demonstrate that such contributions can be at least equally important and scale as $\mathcal{O}(N_{\mathbf{k}}^{-1})$. We propose the staggered mesh method that uses a different set of quadrature nodes for the trapezoidal quadrature, which allows us to completely avoid the first source of the error. Numerical evidence shows that the staggered mesh method is particularly advantageous over the standard method for quasi-1D systems and systems with symmetries, which reduces the contribution from the second error source. We expect that the new approach can also be useful for correlation energy calculations beyond the MP2 level, such as higher levels of perturbation theories and couple clustered theories.

Acknowledgement

This work was partially supported by the Air Force Office of Scientific Research under award number FA9550-18-1-0095 (X.X.,L.L.), by the Department of Energy under Grant No. DE-SC0017867, and by the National Science Foundation under Grant No. DMS-1652330 (L.L.), and by the China Scholarship Council under File No. 201906040071. (X.L).

References

- (1) Marsman, M.; Grüneis, A.; Paier, J.; Kresse, G. Second-order Møller–Plesset perturbation theory applied to extended systems. I. Within the projector-augmented-wave formalism using a plane wave basis set. *The Journal of Chemical Physics* **2009**, *130*, 184103.

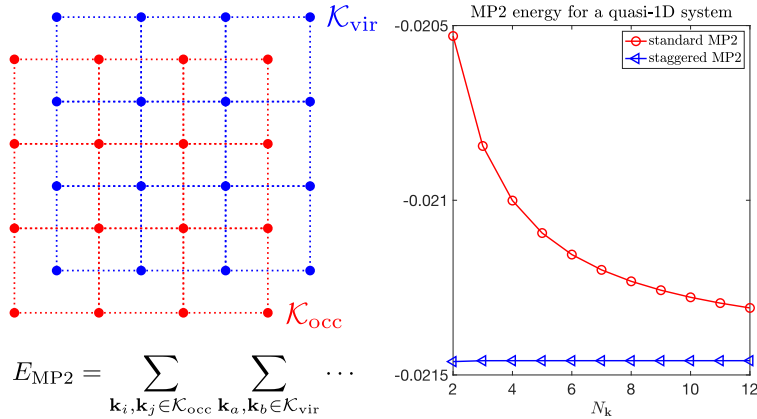


Figure 9: TOC

- (2) Grüneis, A.; Marsman, M.; Kresse, G. Second-order Møller–Plesset perturbation theory applied to extended systems. II. Structural and energetic properties. *The Journal of Chemical Physics* **2010**, *133*, 074107.
- (3) Müller, C.; Paulus, B. Wavefunction-based electron correlation methods for solids. *Phys. Chem. Chem. Phys.* **2012**, *14*, 7605–7614.
- (4) Schäfer, T.; Ramberger, B.; Kresse, G. Quartic scaling MP2 for solids: A highly parallelized algorithm in the plane wave basis. *J. Chem. Phys.* **2017**, *146*, 104101.
- (5) McClain, J.; Sun, Q.; Chan, G. K. L.; Berkelbach, T. C. Gaussian-based coupled-cluster theory for the ground-state and band structure of solids. *J. Chem. Theory Comput.* **2017**, *13*, 1209–1218.
- (6) Gruber, T.; Liao, K.; Tsatsoulis, T.; Hummel, F.; Grüneis, A. Applying the coupled-cluster ansatz to solids and surfaces in the thermodynamic limit. *Phys. Rev. X* **2018**, *8*, 021043.
- (7) Booth, G. H.; Grüneis, A.; Kresse, G.; Alavi, A. Towards an exact description of electronic wavefunctions in real solids. *Nature* **2013**, *493*, 365–370.
- (8) Liao, K.; Grüneis, A. Communication: Finite size correction in periodic coupled cluster theory calculations of solids. *J. Chem. Phys.* **2016**, *145*, 141102.

- (9) Mihm, T. N.; McIsaac, A. R.; Shepherd, J. J. An optimized twist angle to find the twist-averaged correlation energy applied to the uniform electron gas. *The Journal of Chemical Physics* **2019**, *150*, 191101.
- (10) Mihm, T. N.; Yang, B.; Shepherd, J. J. Power laws used to extrapolate the coupled cluster correlation energy to the thermodynamic limit. *arXiv, 2007.11696* **2020**,
- (11) Chiesa, S.; Ceperley, D. M.; Martin, R. M.; Holzmann, M. Finite-size error in many-body simulations with long-range interactions. *Phys. Rev. Lett.* **2006**, *97*, 6–9.
- (12) Lin, C.; Zong, F.; Ceperley, D. M. Twist-averaged boundary conditions in continuum quantum Monte Carlo algorithms. *Physical Review E* **2001**, *64*, 016702.
- (13) Broqvist, P.; Alkauskas, A.; Pasquarello, A. Hybrid-functional calculations with plane-wave basis sets: Effect of singularity correction on total energies, energy eigenvalues, and defect energy levels. *Physical Review B* **2009**, *80*, 085114.
- (14) Shepherd, J. J.; Henderson, T. M.; Scuseria, G. E. Coupled cluster channels in the homogeneous electron gas. *The Journal of Chemical Physics* **2014**, *140*, 124102.
- (15) Gell-Mann, M.; Brueckner, K. A. Correlation energy of an electron gas at high density. *Physical Review* **1957**, *106*, 364.
- (16) Hättig, C.; Klopper, W.; Köhn, A.; Tew, D. P. Explicitly correlated electrons in molecules. *Chemical Reviews* **2012**, *112*, 4–74.
- (17) Grüneis, A.; Shepherd, J. J.; Alavi, A.; Tew, D. P.; Booth, G. H. Explicitly correlated plane waves: Accelerating convergence in periodic wavefunction expansions. *The Journal of Chemical Physics* **2013**, *139*, 084112.
- (18) Sun, Q.; Berkelbach, T. C.; Blunt, N. S.; Booth, G. H.; Guo, S.; Li, Z.; Liu, J.; McClain, J. D.; Sayfutyarova, E. R.; Sharma, S., et al. PySCF: the Python-based

- simulations of chemistry framework. *Wiley Interdisciplinary Reviews: Computational Molecular Science* **2018**, *8*, e1340.
- (19) Lyness, J. An error functional expansion for N -dimensional quadrature with an integrand function singular at a point. *Mathematics of Computation* **1976**, *30*, 1–23.
- (20) Drummond, N. D.; Needs, R. J.; Sorouri, A.; Foulkes, W. M. C. Finite-size errors in continuum quantum Monte Carlo calculations. *Phys. Rev. B* **2008**, *78*, 1–19.